Available online at www.sciencedirect.com
SCIENCE DIRECT®
Journal of Sound and Vibration 269 (2004) 467–488
JOURNAL OF SOUND AND VIBRATION
www.elsevier.com/locate/jsvi

Parametric study of a drum-like silencer

Lixi Huang

Department of Mechanical Engineering, The Hong Kong Polytechnic University, Kowloon, Hong Kong

Received 14 January 2002; accepted 20 December 2002

Abstract

An optimization study is carried out for a silencer consisting of two side-branch, rectangular cavities covered by membranes highly stretched in the direction of the duct axis. Stopband is defined as the range of frequency where the transmission loss is everywhere higher than the peak value of that in an expansion chamber which occupies three times as much cavity volume as does the present silencer. The logarithmic bandwidth is optimized with respect to the length-to-depth ratio of the cavity, the mass and the tension of the membrane. For two cavities each with a dimensionless volume of 5 (the duct height being the length scale), the optimal cavity aspect ratio is 6.6, and the lower stopband frequency is 0.09 times the first cut-on frequency of the rigid duct. This is compared favourably with the traditional duct lining modelled as an equivalent fluid. As the membrane mass increases, the stopband shifts to lower frequencies but it also narrows. The widest stopband is around 1.6 octaves for a massless membrane. The membrane tension plays a delicate role of setting the intervals between adjacent spectral peaks.

1. Introduction

Fibrous duct lining is a very mature and reliable technique which works well for the medium- to high-frequency range. However, its ineffectiveness in the low-frequency range, such as that below 200 Hz, calls for alternative treatments. More importantly, there has been increasing environmental concern about the deposition and accumulation of dusts in the pores of the porous material. A periodical cleaning of the lining would be rather costly and indeed tedious. In fact, there are already public concerns of bacteria breading in the centralized ventilation systems of ordinary commercial buildings. The use of porous material for noise- or heat-insulation purposes might have contributed to an indoor air quality which is often worse than outdoors. There are also places such as operation theatres, where high hygienic requirement forbids the use of such materials. The need of controlling low-frequency noise in an environment-friendly manner

E-mail address: lixi.huang@polyu.edu.hk (L. Huang).

0022-460X/03/$ - see front matter
doi:10.1016/S0022-460X(02)01642-5

calls for a fibreless approach. A team of acousticians led by Fuchs [1] have been very successful in achieving this goal, both technically and commercially. Sharing exactly the same technical goal, the present author conducted a preliminary theoretical study [2] on the use of tensioned membranes as part of the duct walls to reflect the grazing incident noise. Focusing on the mechanism of fluid–structure interaction inside the main duct, the effect of fluid external to the membrane was excluded. In the present study, the membranes are backed by rigid-walled cavities, as should be the case in a practical silencer design, and the tension required turns out to be very high in order to achieve a broadband performance in the low- to medium-frequency range. The membrane response resembles that of a drum, and the device is described as being 'drum-like', or simply a 'drum silencer'. Details are given in the present article to show how the transmission loss spectrum of a drum silencer varies with respect to the cavity shape for a given volume, and how the membrane properties determine the performance. It is shown later that, for a typical duct height of 17 cm, and a two-dimensional side-branch cavity 17 cm deep and 85 cm long, the optimal cavity shape is around 97 cm in length and 15 cm in depth, and the membrane can be made by an aluminium foil of 0.077 mm thickness. Before proceeding, it is perhaps informative to review the membrane properties used in related studies.

The British Broadcasting Corporation (BBC) was among the first to use membrane absorbers for their studios on a large scale, see Ref. [3]. They pioneered a modular approach to the panel sound absorbers. The modules are designed with a face area of 2 ft by 3 ft, a cavity consisting of 7 in air space in front of the rigid wall, and 1 in of semi-rigid glass fibre of density 3 $\mathrm{lb/ft^3}$. The cover membrane is normally perforated. A $\frac{1}{4}$ in thick membrane with 5% perforation gives peak performance in the range of 300–400 Hz, while a true bass absorber is obtained with a cover of 0.5% perforation. If essentially neutral modules (without sharp peaks) are desired, a $\frac{3}{8}$ or $\frac{1}{4}$ in plywood can be used yielding an absorption coefficient with a peak value of 0.3 at 70 Hz. There have been continuous efforts to predict analytically the performance of similar membrane absorber designs. For example, Ford and McCormick [4] studied the absorption characteristics of a stiff panel made of 0.2 mm thick aluminium backed by a shallow cavity of 3 cm depth. It was reported that the choice of the stiff membrane was made after repeated failures to use thin membranes. The advantages of using a stiff panel absorber were that it can have more than one resonant frequency and hence more than one absorption band, and that it was easy to construct offering a wide choice of materials. The disadvantages were that the stiffness of the panel reduced the width of the absorption bands and that the damping can only be optimized for one of the resonant frequencies. Sakagami and his colleagues have carried out extensive studies on similar topics, both analytically and experimentally. Their earlier models were based on infinite impervious membrane using the Helmholtz integral formulation, see, for example, Ref. [5]. These models were later extended to permeable membranes [6], and to finite poroelastic plate [7]. The thickness of the membrane was such that the membrane-to-cavity mass ratio ranged from unity to around 20 in their experiments. Bosmans et al. [8] investigated the sound absorption by a stretched PVC ceiling with a cavity infill made of mineral wool or polyurethane foam. The typical rig consisted of a 0.15 mm PVC foil, stretched over an area of 3.17 m by 3.17 m, with 15 cm deep cavity in which there was a porous, 2 cm thick layer. The mass ratio of the foil to the cavity air was about 0.92. The tensile force applied gave an in vacuo flexural wave speed of around 60 m/s. This force was deemed insignificant when compared with the foil inertia and cavity stiffness. Ackermann et al. [9] described the details of their innovative, all-metal membrane absorber which

can be used in hazardous industrial environment or applications with high hygienic standards. The absorber was made by a host of baffled Helmholtz resonators. A typical resonator unit consisted of a rigid cavity of 5 cm depth with a perforated panel of 0.2 mm aluminium, covered by a thin aluminium membrane (0.1 mm) at a distance of less than 1 mm from the perforated one. The result was a broadband performance in the low- to medium-frequency range. Kang and Fuchs [10] modelled their cavity-backed porous membrane as a parallel connection of apertures and the membrane. In their validation experiments, an impedance tube of 20 cm by 20 cm in cross-section was used to measure the absorption by a 0.17 mm thick glassfibre textile backed by a cavity of 10 cm depth. Again, broadband sound absorption performance was achieved.

In summary, the thickness of membranes used in all these studies is comparable to that of the current study although much thicker membranes have also been tested mainly for room acoustics purposes. Tensile stress was applied in one case but its effect was found negligible. Bending stiffness in the relatively thick membrane played an important role, but the cavity stiffness had always been more dominant. Damping mechanisms were essential parts of a system and it was achieved through filling sound absorption materials in the cavity and/or using perforated membranes. The cavity was always compact compared with the quarter-wavelength in all studies. Contrasting with all these previous studies, the drum silencer here uses a non-compact, thin membrane under high tension. Damping is not a key element of the system. It is found that the crucial mechanism for the broadband performance is the excitation of multiple resonant peaks with suitable intervals between these peaks. If the membrane response is expanded in terms of its in vacuo modes for the simply supported configuration, the contribution of the second in vacuo mode is found to be very significant, and indeed unique for the present system. This mode is a non-volume-displacing mode, and the cavity is not stiff. The second mode response supplements that of the first mode, the latter being limited by the stiffness of the cavity air. The so-called suitable interval between spectral peaks is found through an optimization process. The parameters to be varied include the aspect ratio of the cavity for a given volume, the membrane-to-air mass ratio, and the tensile stress applied on the membrane. To put the performance of the drum silencer in a practical perspective, the normalized spectra of duct lining are studied with a certain performance criterion. This is described in the next section, followed by a brief study of duct lining with various properties of sound absorption materials. These results then serve as a reference for judging how the drum silencer performs in different geometrical shapes.

2. Formulation

This section outlines the theoretical formulation used to predict the transmission loss of the drum silencer. It begins with the description of a general theoretical model for the coupled dynamics of membrane with and without sound absorption material in the cavity. The key procedure of solution is given in the second subsection. Details of the fluid–membrane coupling for one specific membrane–cavity configuration is described in Ref. [11], and experimental validation of the theory can be found in Ref. [12]. The last subsection explains the performance criterion for the drum silencer and explores how traditional duct lining (without membrane cover) measures up to this performance criterion.

2.1. Theoretical model and normalization scheme

As shown in Fig. 1, a rectangular duct is modelled by a two-dimensional channel while retaining the liberal use of the word 'duct'. Part of the duct walls are lined with two identical, stretched membranes, and each membrane is backed by a rigid-walled cavity. If the membranes are removed, the configuration reduces to a simple expansion chamber. When excited by an incident wave, the membranes vibrate and the left-going sound radiation forms the reflection wave thus reducing the transmitted wave. The action of the highly stretched membrane resembles that of a drum skin, hence the name drum silencer. The cavity is used to prevent break-out noise.

Before quantifying the membrane dynamics, a normalization scheme is introduced to simplify the procedure as well as to identify controlling parameters. All dimensional variables are denoted by an asterisk and their dimensionless counterparts are given the same symbol without these asterisks. Variables related to the cavities are given an extra subscript 'c', and those of sound absorption material '*sam*'. Three basic quantities are used for normalization. They are the duct height h^* as the length scale, air density ρ_0^*, and the speed of sound in free space with air, c_0^*, quantities associated with free space air being identified by a subscript '0'. The redundant dimensionless variables $h = h^*/h^* = 1$ and $c_0 = c_0^*/c_0^* = 1$ are retained in some formulas for convenient generalization to wave propagation in isotropic sound absorption materials modelled as an equivalent fluid with complex speed of sound. The combination of the length scale h^* and the velocity scale c_0^* gives the time scale of h^*/c_0^*, while the acoustic impedance and pressure scales are, respectively, $\rho_0^* c_0^*$ and $\rho_0^* {c_0^*}^2$. The normalization of frequency f^*, angular frequency ω^*, and a wavenumber in a duct k_n^*, are as shown below:

$$f = f^* h^*/c_0^*, \quad \omega = \omega^* h^*/c_0^* = 2\pi f, \quad k_n = k_n^* h^*. \tag{1}$$

The dimensionless first cut-on frequency of the rigid-walled duct is $f = 0.5$. The membrane has a dimensional mass per unit area m^*, stretched under a tensile force T^* per unit length in the third direction. The membrane-to-air mass ratio m and the dimensionless tension T are

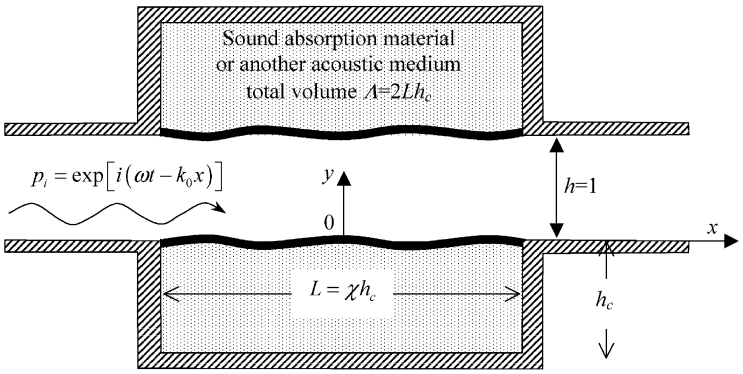

Fig. 1. Configuration of cavity filled with sound absorption material or another acoustic medium. The total volume Λ refers to the two cavities.

defined by

$$m = \frac{m^*}{\rho_0^* h^*}, \quad T = \frac{T^*}{\rho_0^* c_0^{*2} h^*}, \tag{2}$$

and both are made to vanish for normal duct lining without cover membranes.

The configuration in Fig. 1 is labelled by dimensionless variables. The cavity has a depth h_c and the membrane has a length L. The cavities can be either empty or filled with sound absorption materials. The total volume of the two cavities is denoted Λ while the length-to-depth aspect ratio, χ. The geometrical relationships are

$$\Lambda = 2Lh_c, \ \ \chi = L/h_c, \quad L = \sqrt{\Lambda\chi/2}, \ \ h_c = \sqrt{\Lambda/(2\chi)}. \tag{3}$$

The basic procedure of solving the couple dynamics of the membrane follows that of the earlier study [2] although the effect of the cavity air was ignored. The main steps are described here briefly, while formulations unique to the current model are given in more detail. The dynamics of the fluid–structure coupling is described by the following equation for membrane displacement η, which is related to the vibration velocity by $V = \mathrm{i}\omega\eta$ when considering incident sound of time dependency $\mathrm{e}^{\mathrm{i}\omega t}$:

$$m\partial^2\eta/\partial t^2 - T(1 + \mathrm{i}\sigma)\partial^2\eta/\partial x^2 + \Delta p + p_i = 0, \tag{4}$$

where

$$p_i = \mathrm{e}^{\mathrm{i}(\omega t - k_0 x)}, \tag{5}$$

is the known incident wave pressure, Δp is the self-induced loading over the two sides of the membrane caused by its own vibration, and σ is the loss factor of the membrane, which is explained as follows. The exact mechanism of damping in a tensioned membrane is rather complex. In addition, energy loss caused by the friction at the two edges, $x = \pm L/2$, might be more important than the distributed damping over the bulk membrane length. However, accurate modelling of the damping mechanism is beyond the scope of the current study. The emphasis here is to examine whether a reasonably high level of damping can be translated into an advantage in terms of the overall transmission loss. If it can, efforts can be made in the direction of increasing structural damping by means of sandwich designs, etc. It is for this purpose that the above rudimentary damping model is put forward in the following analyses. It is obvious that the usual concept of loss factor incorporated as the imaginary part of a complex Young's modulus is not suitable here. Alternatively, the traditional dashpot concept would yield an inertia term like $-m\omega^2\eta(1 - \mathrm{i}\sigma)$, in which the damping term represents the energy loss from a flat membrane undergoing a heaving motion like a piston. Such a piston model can be adopted on conceptual basis, but it is felt that it would be more appropriate to model the structural damping based on the shearing motions experienced by a vibrating membrane treated as a plate. A loss factor attached to the curvature term in the form of $T\eta_{xx}(1 + \mathrm{i}\sigma)$ is adopted as a rudimentary damping model for the present study. Strictly speaking, a constant value of σ for all frequencies is unlikely to be satisfactory for any damping model, but, judging from the results of the following calculations, a model of constant σ can still serve the illustration purpose. As far as the transmission loss is concerned, the quantitative difference between the results of this model and those of a piston model with the same value of σ is found to be insignificant.

The Galerkin procedure can be followed to solve the above dynamics equation in terms of a modal expansion for a simply supported membrane,

$$V = \sum_{j=1}^{\infty} V_j \sin(j\pi\xi), \quad V_j = 2\int_0^1 V \sin(j\pi\xi)\,\mathrm{d}\xi, \quad \xi = x/L + \tfrac{1}{2}. \tag{6}$$

The main task in doing so is to relate the fluid loading Δp with the vibration velocity V through a modal impedance matrix $\{Z_{jl}\}$ as shown below:

$$\Delta p = \sum_{l=1}^{\infty}\left(\sum_{j=1}^{\infty} V_j Z_{jl}\right)\sin(l\pi\xi), \tag{7}$$

where the single mode impedance Z_{jl} is defined as the lth fluid loading coefficient caused by the vibration of the jth in vacuo mode of unit amplitude, $\sin(j\pi\xi)$. Details of finding Z_{jl} are given in the next subsection. Substitution of Eq. (7) into Eq. (4) gives a truncated set of linear equations:

$$\begin{bmatrix} Z_{11}+\mathscr{L}_1 & Z_{12} & \cdots & Z_{1N} \\ Z_{21} & Z_{22}+\mathscr{L}_2 & \cdots & Z_{2N} \\ \cdots & \cdots & \cdots & \cdots \\ Z_{N1} & Z_{N2} & \cdots & Z_{NN}+\mathscr{L}_N \end{bmatrix} \begin{bmatrix} V_1 \\ V_2 \\ V_3 \\ \vdots \\ V_N \end{bmatrix} + \begin{bmatrix} I_1 \\ I_2 \\ I_3 \\ \vdots \\ I_N \end{bmatrix} = 0, \tag{8}$$

where I_j is the modal coefficient of the incident wave, and $\mathscr{L}_j$ is mainly determined by the membrane property:

$$I_j = \int_0^1 p_i 2\sin(j\pi\xi)\,\mathrm{d}\xi = 2j\pi \mathrm{e}^{\mathrm{i}k_0 L/2}\left[\frac{1-\mathrm{e}^{\mathrm{i}(-k_0L+j\pi)}}{(j\pi)^2-(k_0L)^2}\right],$$
$$\mathscr{L}_j = \left[m\mathrm{i}\omega + \frac{T}{\mathrm{i}\omega}\left(\frac{j\pi}{L}\right)^2(1+\mathrm{i}\sigma)\right]. \tag{9}$$

Eqs. (8) can be solved for the vibration velocity coefficients V_j by standard matrix inversion techniques like Gaussian elimination.

2.2. Impedance matrix and membrane dynamics

The task of finding the modal impedance Z_{jl} is one in which, unlike the coupled membrane dynamics, the membrane vibration is specified, and the loading is customarily called the radiation pressure. The formulation with one vibrating membrane is given below, and the effect of the opposite, identical membrane can be easily taken into account by regarding the centreline of the duct as a rigid wall. The radiation pressure on the membrane surface facing the main duct, denoted p_{+rad}, can be found by the summation over all duct acoustics modes, ψ_n, as shown below

(see, for example, Ref. [13]):

$$p_{+rad}(x,y,t) = \frac{\rho_0}{2h}\sum_{n=0}^{\infty} c_n\psi_n(y/h)\int_{-L/2}^{+L/2}\psi_n(y'/h)V(x',y',t) \times \quad [\mathrm{H}(x-x')\mathrm{e}^{-\mathrm{i}k_n(x-x')} + \mathrm{H}(x'-x)\mathrm{e}^{+\mathrm{i}k_n(x-x')}]\,\mathrm{d}x',$$

$$\psi_n(y/h) = \sqrt{2-\delta_{0n}}\cos(n\pi y/h), \quad k_n = \frac{\omega}{c_n}, \quad c_n = \frac{\mathrm{i}c_0}{\sqrt{(n\pi/k_0h)^2-1}}, \tag{10}$$

where c_n and k_n are, respectively, the phase speed and wavenumber of the nth duct acoustics mode, H is the Heaviside function, δ_{0n} is the Kronecker delta. The integration is carried out over the source surface: $x' \in [-L/2, L/2], y' = 0$. The pressure on the cavity side is found in two steps. First, the cavity is regarded as a channel of infinite length in which the membrane vibration radiates sound of pressure p_{-rad} in a way identical to p_{+rad}. Second, the effect of the two vertical walls at $x = \pm L/2$ is taken into account by enforcing the rigid wall boundary conditions there. Eq. (10) can be adapted for p_{-rad} when $\rho_0 = 1$ and $c_0 = 1$ are replaced by the corresponding medium properties inside the cavity, denoted, respectively, as ρ_{sam} and c_{sam}, the vibration velocity V is replaced by $-V$, and h by h_c. The reflection wave loading p_{-ref} is also expressed as a summation of duct acoustics modes ψ_n, like in Eq. (10), except that the two Heaviside functions are replaced by two constants, A and B,

$$p_{-ref}(x,y,t) = \frac{\rho_{sam}}{2h_c}\sum_{n=0}^{\infty} c_{nc}\psi_n(y/h_c)\int_{-L/2}^{+L/2}\psi_n(y'/h_c) \times \quad [-V(x',y',t)] \times [A\mathrm{e}^{-\mathrm{i}k_{nc}(x-x')} + B\mathrm{e}^{+\mathrm{i}k_{nc}(x-x')}]\,\mathrm{d}x',$$

$$c_{nc} = \frac{\mathrm{i}c_{sam}}{\sqrt{(n\pi/k_{sam}h_c)^2-1}}, \quad k_{nc} = \frac{\omega}{c_{nc}}, \quad k_{sam} = \frac{\omega}{c_{sam}}, \tag{11}$$

which are found by the rigid wall boundary conditions at $x = \pm L/2$,

$$\left.\frac{\partial(p_{-rad}+p_{-ref})}{\partial x}\right|_{x=\pm L/2} = 0 \rightarrow A = \frac{\mathrm{e}^{\mathrm{i}k_{nc}(L-2x')}+1}{\mathrm{e}^{\mathrm{i}k_{nc}(2L)}-1}, \; B = \frac{\mathrm{e}^{\mathrm{i}k_{nc}(L+2x')}+1}{\mathrm{e}^{\mathrm{i}k_{nc}(2L)}-1}. \tag{12}$$

Note that an additional subscript 'c' denotes cavity.

Both ρ_{sam} and c_{sam} are complex quantities, and are functions of frequency. The typical functionality of glassfibre described in Ref. [14] is used in the following analysis. The controlling parameter for sound absorption material can be either porosity or flow resistivity, R^*_{sam}. The latter is used and is normalized as follows:

$$R_{sam} = (R^*_{sam}h^*)/(\rho^*_0c^*_0). \tag{13}$$

For a typical density where $R^* = 30\ \mathrm{kN\,s/m^4}$ used in a duct of 20 cm height, R_{sam} is around 14. It will be shown in the following examples that the optimal value is much less than this for best low-frequency performance.

Once the vibration velocity is found via modal vibration coefficients V_j through solving the coupled dynamics equation, Eq. (4), the reflected wave, denoted as p_r, can be found by evaluating

the radiated wave into the far left from Eq. (10), while the transmitted wave, p_t, is found by the superposition of the incident wave, p_i, with the radiation into the far right, also from Eq. (10). The coefficients of energy flux reflection, β, wave absorption, α, and the transmission loss, TL, can be evaluated as follows:

$$p_r = p_{+rad}|_{x\to-\infty}, \quad p_t = p_{+rad}|_{x\to+\infty} + p_i,$$
$$\beta = \left|\frac{p_r}{p_i}\right|^2, \quad \alpha = 1-\beta-\left|\frac{p_t}{p_i}\right|^2, \quad TL = 20\log_{10}\left|\frac{p_i}{p_t}\right|. \tag{14}$$

The complex amplitude of the reflected sound, p_r, is the sum of contributions made by all individual membrane vibration modes, which is found as follows with the help of Eq. (10):

$$p_r = \frac{1}{2}\int_{-L/2}^{+L/2} V(x')\mathrm{e}^{-\mathrm{i}k_0x'}\,\mathrm{d}x' = \sum_{j=0}^{\infty} V_jR_j, \quad R_j = \frac{1}{2}\int_{-L/2}^{+L/2} \sin(j\pi\xi')\mathrm{e}^{-\mathrm{i}k_0x'}\,\mathrm{d}x', \tag{15}$$

where R_j is the complex amplitude of the reflected sound by the induced vibration of the jth mode with unit amplitude. Since the summation of complex amplitudes can be seen as vectorial sum on the real–imaginary plane, the contributions from all odd modes, $j = 1, 3, 5, \ldots$, towards reflected wave can be grouped together as $V_{odd}R_{odd}$, and those from the even modes $V_{even}R_{even}$. Their interference can be characterized by an index defined as follows:

$$\Gamma_{odd,even} = \cos\theta, \tag{16}$$

where θ is the phase angle difference between the two complex amplitudes. When $\theta\to\pi$, destructive interference results.

2.3. Performance criterion and duct lining

It is well-known that duct lining performs well in the range of medium-to-high frequencies, and membrane absorbers target at low-to-medium frequencies. It is necessary to specify exactly what is meant by 'medium frequency' and what measures up to the so-called 'good performance'. For this purpose, a performance criterion is needed, and the lowest frequency at which the criterion is met for the duct lining may be seen as a reference 'medium frequency' separating the low and high frequencies in the current context.

When the two cavities are put together, the total volume occupied, Λ, is regarded as a kind of 'cost'. A reference expansion chamber is chosen to be one in which $\chi = L/h_c = 2, L = 2h_c = \sqrt{\Lambda}$, so the expansion ratio of the reference expansion chamber is $1 + 2h_c = 1 + \sqrt{\Lambda}$. Since the performance of the drum silencer is expected to be much better than that of empty expansion chambers, the criterion of satisfactory, or threshold, transmission loss is set as the peak value for an expansion chamber with an added volume which is three times the actual added volume used, i.e., 3Λ. The ratio of expansion becomes $1 + \sqrt{3\Lambda}$. The peak performance occurs when the chamber is a quarter-wavelength long. The plane-wave theory gives this threshold transmission loss, TL_{cr}, and the dimensionless peak frequency f_{peak}:

$$TL_{cr} = 10\log_{10}\left[1 + \frac{1}{4}(a_3 - a_3^{-1})^2\right], \quad a_3 = 1 + \sqrt{3\Lambda}, \quad f_{peak} = \frac{1}{4\sqrt{3\Lambda}}. \tag{17}$$

For an added volume of $\Lambda = 10$, the result is $TL_{cr} = 10.4$ dB and $f_{peak} = 0.0456$. Notice that, if a lower aspect ratio χ is chosen for the reference expansion chamber, the chamber would become very short with high area expansion ratio. TL_{cr} calculated according to the plane-wave theory will be very high. In fact, the plane-wave theory breaks down for short expansion chambers which behave more like resonators with sharp spectral peaks. The choice of $\chi = 2$ is already too low for TL_{cr} to hold accurately, but it is believed to be an appropriate one just for the purpose of setting TL_{cr}.

Before studying the optimal cavity shape for the drum silencer, it is of interest to see how traditional duct lining measures up to this criterion. Notice that, for a lining within such finite cavities, sound reflections at the upstream and downstream junctions of the cavities will certainly make a significant contribution. The performance of the traditional duct lining is calculated by treating the sound absorption material in the two cavities as equivalent fluid and allowing the membrane mass to vanish.

The cavity geometry is first assumed to be $h_c = 1, L = 5$, for which $TL_{cr} = 10.41$ dB, and the effect of change χ is described next. The spectra of transmission loss, TL, and the sound energy reflection coefficient, β, are shown in Fig. 2 in terms of dimensionless frequency $f = f^*h^*/c_0^*$ for

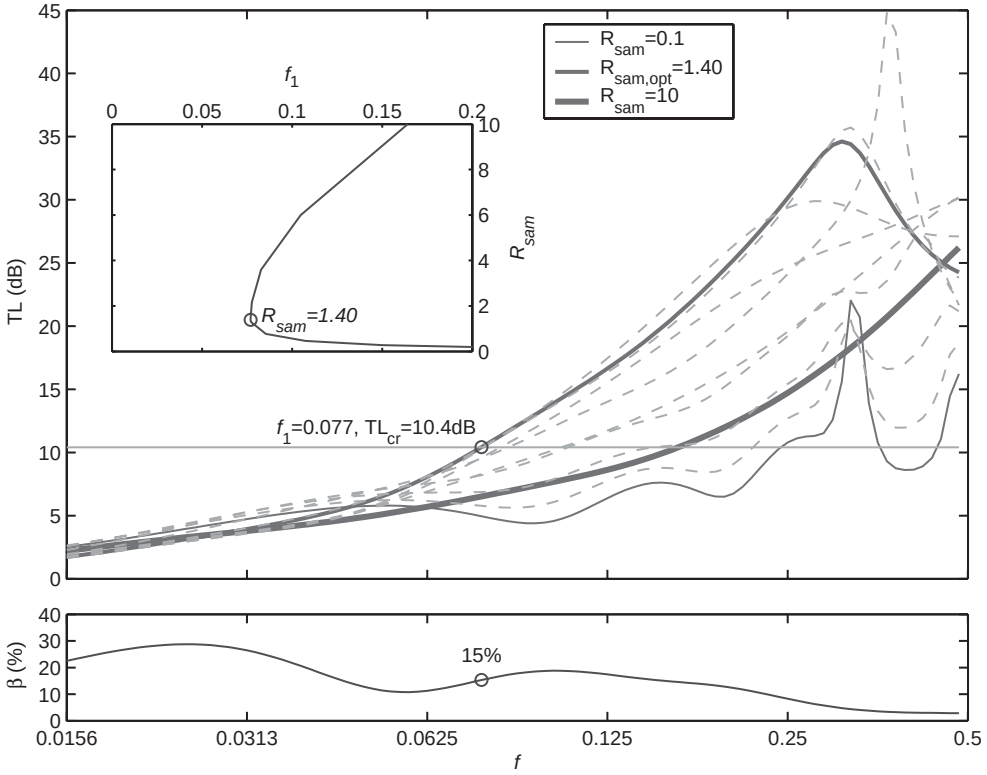

Fig. 2. Spectra of duct lining filling two cavities of depth $h_c = 1$ and length $L = 5$. Each dashed line in the main picture corresponds to one value of flow resistivity R_{sam} which increases from 0.1 (thin solid line) to 10 (thickest solid line) in equal logarithmic increment. The solid line of medium thickness is the optimal curve for $R_{sam} = 1.4$ which produces the lowest value of lower stopband limit f_1. The insert shows the variation of f_1 with respect to R_{sam}. The lower spectrum of β is the reflection coefficient for $R_{sam} = 1.7$.

various values of dimensionless flow resistivity. It shows that the lining performs better in the region of higher frequencies. The crucial result in this case is the lower boundary of the stopband, f_1, for which a very low value is desired. The variation of f_1 with flow resistivity R_{sam} is shown in an insert figure. It can be seen that the performance in this regard is bad for extremely low and high values of R_{sam}, whose spectra are indicated in the main figure by the thinnest and the thickest lines, respectively. The lowest $f_1 = 0.077$ is found with a lining of $R_{sam} = 1.4$, and the optimal TL spectrum is shown as the solid line of medium thickness. The peak in the insert is rather sharp, indicating a strong dependency of the low-frequency performance on the exact flow resistivity. The contribution of sound reflection in this case is shown in the lower figure, in which $\beta = 15\%$ is marked for the frequency of $f_1 = 0.077$. A peak in the optimal TL curve appears around frequency 0.3, which is an indication of resonance in the direction of the cavity depth. The reason why the performance for $R_{sam} = 1.4$ is better than that of $R_{sam} = 10$ for $f < 0.5$ is that, in the former case, the standing wave between the air–lining interface and the lower cavity wall allows maximum particle velocity to be produced in the material. Part of the reactive nature of the shallow duct lining is also obvious in the sharpness of the peak in the insert picture.

For each cavity geometry, the best f_1 and R_{sam} can be found. The variation of these with respect to the cavity depth h_c for a given cavity volume of $\Lambda = 10$ are shown in Fig. 3. Fig. 3(a) shows that

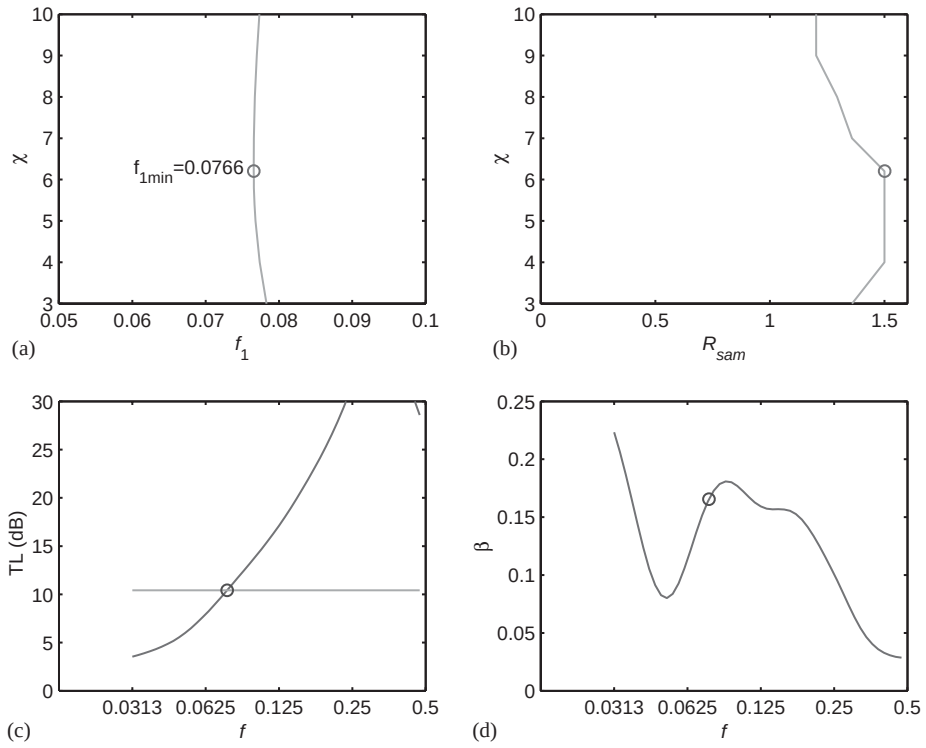

Fig. 3. Optimal cavity depth for duct lining which occupies the added volume of $\Lambda = 10$: (a) the variation of f_1 with the cavity depth h_c; (b) the optimal flow resistivity for each cavity depth; (c) and (d) the TL spectrum and the reflection coefficient for the optimal aspect ratio $\chi = 6.2$. The open circles in (a) and (b) mark the optimal cavity geometry, while those in (c) and (d) mark the lower frequency band.

the performance of the cavity barely changes with the cavity depth, but a minimum of $f_1 = 0.0766$ is identified with $h_c = 0.9$. Fig. 3(b) shows that deeper cavity requires higher flow resistivity. Fig. 3(c) is the spectrum of the optimal cavity depth of 0.9 with the optimal flow resistivity of 1.3. The contribution of reflection beyond the frequency of f_1 is around 15%. It is concluded that cavities filled with sound absorption material of a suitably chosen property can achieve satisfactory performance down to the frequency of 0.077. This frequency limit is not sensitive to the cavity shape, but it is sensitive to the flow resistivity since part of the good performance derives from the cavity depth resonance. The frequency of 0.077 can be seen as a demarcation line for the 'medium' frequency in the present context.

3. Optimal cavity

The drum silencer can be a very simple device for construction, but it does have a lot of variables, for which a parametric study has to begin with most variables fixed. For reasons that become clear later on, the membrane mass is fixed at $m = 1$, the two cavities have a total volume $\Lambda = 10$ without sound absorption materials, and $R_{sam} = 0$. Membrane tension T is a very influential parameter which has to be varied while studying the effect of varying cavity depth h_c or aspect ratio χ. The variation of performance with respect to the volume Λ will be presented towards the end of this section.

3.1. Optimal shape for a given volume

The overall results are first presented in Fig. 4 in a waterfall format. Deep cavities with short membranes have low aspect ratio χ, and their spectra resemble simple Helmholtz resonator.

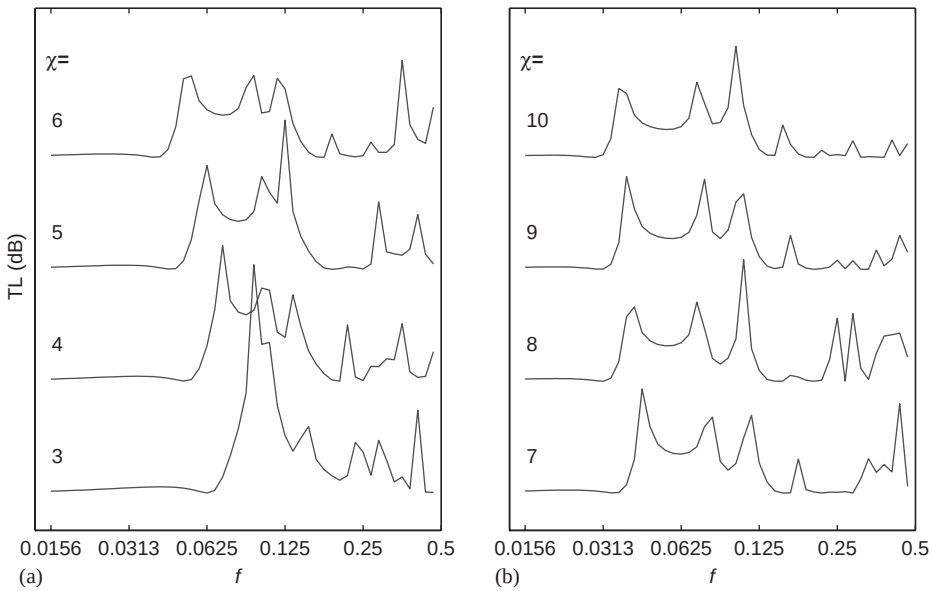

Fig. 4. Variation of spectra with the shape of cavity.

Shallower cavities with longer membranes, on the other hand, have higher aspect ratio and their spectra are broader with peaks spread out in frequency. As χ increases beyond about 7, the dip between the three spectral peaks become progressively serious and the level of TL falls below the criterion value TL_{cr}. The exact bandwidth,

$$f_b = f_2/f_1, \tag{18}$$

and the optimal tension, T_{opt}, are shown in Fig. 5. The cavity depth which yields the widest stopband according to the criterion of Eq. (17) has $\chi = 6.6$, as shown in the peak point of Fig. 5(a). Its spectrum is shown in Fig. 5(c) as thick solid curve. Two other cavity geometries with $\chi = 5.6, 7.8$ are chosen for comparison with the optimal cavity, which are shown together with the optimal cavity depth in three open circles in Fig. 5(a) and (b). The membrane tension used follow the optimal values found for each individual depth, as shown in three open circles in Fig. 5(b). The optimization with respect to T for each cavity geometry will be discussed in the next section. As χ increases, the corresponding optimal tension also increases. It is found that the spectra for the three chosen cases are brought close together if the frequency scale is modified by the membrane length as fL/L_{opt}, where L_{opt} is the length for the optimal cavity depth, $L_{opt} = \sqrt{\chi\Lambda/2} = 5.7$. The results are shown in Fig. 5(c). Through such a frequency modulation, it becomes clear that the

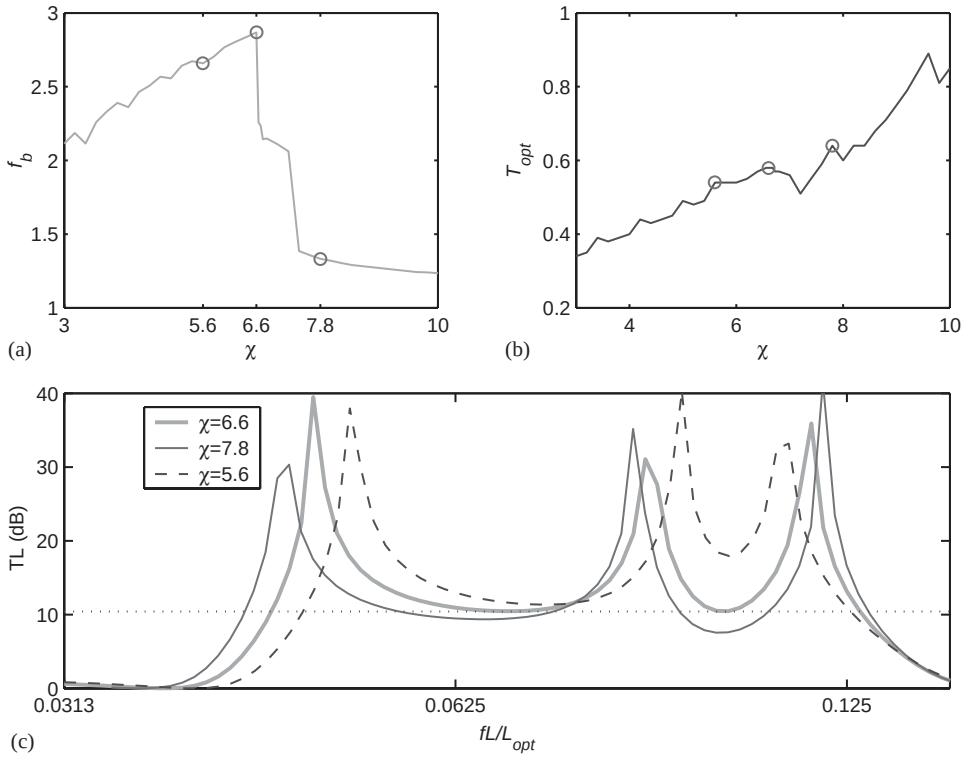

Fig. 5. Optimal cavity geometry: (a) the variation of bandwidth with respect to the cavity depth; (b) the optimal tension calculated for each depth; (c) comparison of the three optimal spectra for three values of cavity depth indicated by three open circles in (a). The frequency scale in this figure is adjusted by the membrane length to facilitate closer comparison.

shallow and longer cavity (thin solid line) is effective over a wider frequency band but the dip between the three TL peaks are rather serious. In fact, for the example shown above, the TL goes below TL_{cr} set by Eq. (17). The so-called optimal geometry is one in which the lowest TL values just touches down to TL_{cr}. On the other hand, deeper and shorter cavity works in a narrower frequency band with better minimal TL. The comparison between the three spectra in Fig. 5(c) serves as a reminder that the variation of the drum silencer performance with cavity depth is rather smooth, and the optimal cavity shape simply depends on the criterion set for the transmission loss.

3.2. Impedance analysis

In order to understand the precise mechanism by which the spectra shift with the cavity shape, it is necessary to analyze the behaviour of each membrane mode. At first sight, this seems rather difficult as Eqs. (8) imply complicated cross-modal coupling. But, as was shown in Ref. [2], for the modal radiation impedance Z_{jl}, there is no coupling between odd and even modes, e.g., $Z_{12} = Z_{21} = 0$, although there is coupling among all odd modes and among all even modes. In addition, it can be easily demonstrated numerically that, at very low frequencies, the odd–odd and even–even couplings are also weak, in which case the coupled equations in Eq. (8) can be approximately solved for the first two modes as follows:

$$V_1 \approx \frac{-I_1}{Z_{11} + \mathscr{L}_1}, \quad V_2 \approx \frac{-I_2}{Z_{22} + \mathscr{L}_2}, \tag{19}$$

where $\mathscr{L}_j$ is the membrane property defined in Eq. (9). The examination of the combined modal impedance $Z_{jj} + \mathscr{L}_j$ can then shed some light on how reflection by a certain mode changes with cavity shape. It is most profitable to analyze the first two modes, $j = 1, 2$, but such analysis would gradually fail as the frequency increases. This pitfall can be avoided by an additional analysis of the lumped odd modes and even modes reflections, $V_{odd}R_{odd}$ and $V_{even}R_{even}$, and their interference index $\Gamma_{odd,even}$ defined in Eq. (16).

The physics of the spectral dependency on cavity depth is now discussed by analyzing the components of the impedance matrix for the three cases shown in Fig. 5(c). The details are shown in Fig. 6 and we recall the notation while explaining the parts of Fig. 6. The total reactance, $X = \mathrm{Im}(Z_j + \mathscr{L}_j)$, of the coupled system of the first and second modes, $j = 1, 2$, are shown in the first and second columns of the figure, respectively. Fig. 6(1a) shows the structural reactance $X_{struct} = \mathrm{Im}(\mathscr{L}_1)$, for which the vertical scale is the same as that of the second mode shown in Fig. 6(2a). A vertical dashed line is shown in all subfigures since it marks an important frequency, the first axial mode of the cavity $f = 1/(2L)$ for the optimal cavity. At this frequency, the cavity reactance becomes singular for the second mode, as shown in Fig. 6(2c), and the response of the even modes are prohibited, as shown in Fig. 6(3c). Focusing now on the comparison between the optimal cavity, shown in thick solid curves, and the shallower cavity, shown in thin solid curves, Fig. 6(1b) shows that the radiation reactance X_{rad}, which derives from the combination of p_{+rad} and p_{-rad}, for the shallow cavity is greater in magnitude, i.e., there is more stiffness caused by the opposite rigid wall on the membrane. This is understood from Eqs. (10) and (11) where the radiation pressure is seen to be scaled with $\chi = L/h_c$. Physically it derives from mass conservation in the sense that all the volume displaced by the membrane of length L produces an equal amount

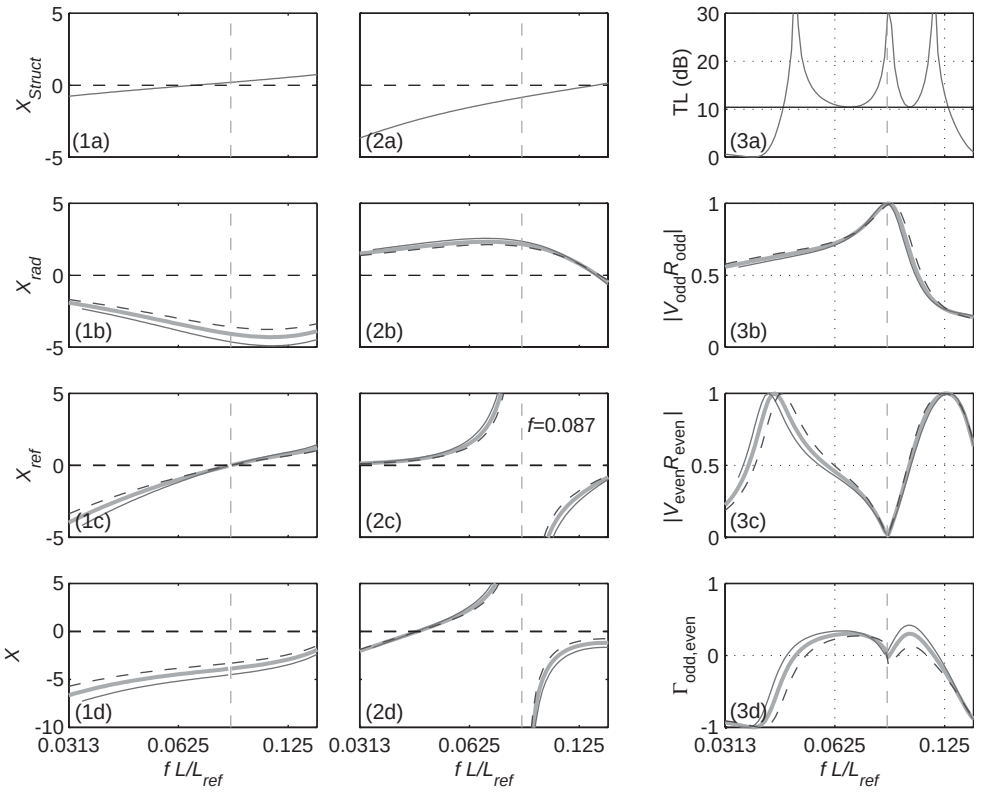

Fig. 6. The effect of cavity depth on the membrane response. The first column is for the first mode analysis, the second column the second mode. The third column deals with the modal reflection coefficients.

of acoustic particle flow elsewhere across the section of height h_c. The enhancement of sound radiation by narrowing the channel is also felt in the magnitude of the sound reflection by the two rigid walls in the cavity, as shown by the greater magnitude of reflection reactance, denoted as X_{ref}, in Fig. 6(1c). Fig. 6(1d) shows that the total reactance X for the shallower cavity is greater, leading to a smaller response from the odd modes, as shown in Fig. 6(3b). The radiation reactance for the second mode is a virtual mass, as shown in Fig. 2(b). For the same reason of higher aspect ratio, $\chi = L/h_c$, shallower cavity produces higher radiation mass and reflection mass, as shown in Fig. 6(2c), leading to a lower even mode response, as shown in Fig. 6(3c). The lower response from all modes leads to lower value of TL over all frequencies within the stopband when compared with that of the optimal cavity. Fig. 6(3d) shows some improvement in the interference index $\Gamma_{odd,even}$ for the shallower cavity, but this does not seem to be sufficient to compensate for the reduced magnitudes of the modal response.

If the TL criterion for the stopband is temporarily abandoned, the shallower cavity apparently has more effective response to a wider frequency band, as shown earlier in Fig. 5(c). The reason why this is the case can be explained here. The main reason is that the even mode response reaches a peak at a lower frequency, as shown in the left-shift of the thin curve in Fig. 6(3c). This shift is partly due to the second mode resonance at a lower frequency as the virtual mass from the

radiation and reflection is enhanced, as shown in Fig. 6(2b) and (2c). The other reason might be that the drastic improvement of interference index in the range of very low frequencies, as shown in Fig. 6(3d). The effect of increasing the cavity depth seems to be exactly opposite and will not be analyzed further.

3.3. Variation with volume

The optimal cavity shape and other parameters are shown in the subfigures on the left column of Fig. 7 as a function of the total cavity volume. The subfigures on the right column are for the duct lining without membrane cover. The parameters are presented in a manner to identify certain constants. Figs. 7(1a) and (2a) compare the limits of the stopband frequency $[f_1, f_2]$, with the quarter-wavelength frequency of expansion chamber of the same length, f_q. Comparing first f_1 between the drum silencer and the duct lining, it is found that f_1 is about the same for the two designs with volume $\Lambda = 5$. But low-frequency performance of the drum silencer surpasses the duct lining as volume increases. At volume 10, the comparison of f_1 stands at 0.0460 versus 0.0672. At volume 15, the comparison becomes 0.0331 versus 0.0573. The lower frequency limit for the drum silencer is 58% of that of the duct lining. The coincidence of f_q and f_1 between the

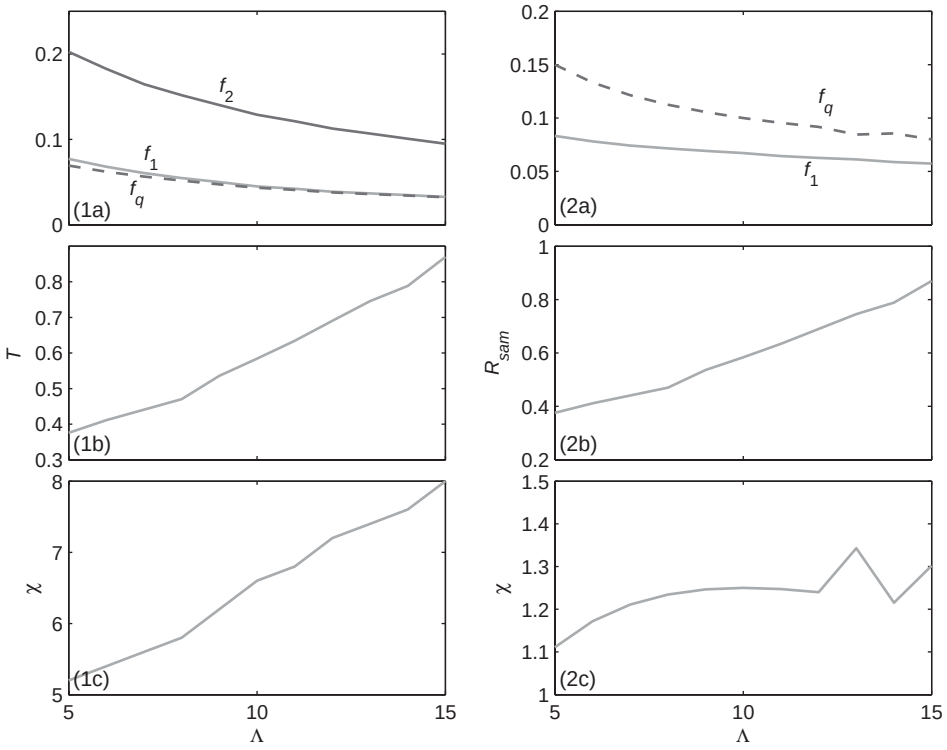

Fig. 7. Variation with cavity volume. The left column is for the drum silencer and the right column is for duct lining without membrane cover. $f_q = 1/(4L)$ is the reference frequency of quarter-wavelength resonance for an expansion chamber of the same length.

expansion chamber and the drum silencer is interesting, but it defies easy interpretation. Fig. 7(1b) shows the optimal tension, which increases with the optimal cavity length. The controlling parameter in duct lining is R_{sam}, and the result is shown in Fig. 7(2b). Larger cavities can afford to have loose sound absorption material. Figs. 7(1c) and (2c) show the aspect ratio of the optimal cavity. The best cavity shape for drum silencer is a long and shallow cavity, with typical ratio of $\chi \in (5, 8)$, while the best for duct lining is $\chi \in (1, 1.5)$. The reference expansion chamber described earlier is a cavity with $\chi = 2$, which is a mid-way between the optimal drum silencer and the optimal duct lining.

4. The effect of membrane properties

The following set of parameters are used in this section,

$$m = 1, \quad \sigma = 0, \quad h_c = 1, \quad L = 5. \tag{20}$$

The effects of membrane tension T, loss factor σ and length L are presented below.

4.1. Optimal tension

The transmission loss spectra for different values of membrane tension are shown in Fig. 8. Fig. 8(a) displays the spectra together with the criterion value TL_{cr} shown for each spectrum, and the value of T for each stacked spectrum is marked on the right-hand side. It can be seen that, as T increases, the resonant frequencies shift towards higher frequencies. The optimal value of T is found to be $T = 0.485$, which can be recognized around $T = 0.5$ where the spectral valleys between the three peaks rise above the horizontal bar of TL_{cr}. The details of this setting are compared with those of two neighbouring design parameters, shown as three open circles in Fig. 8(b) and (c). Fig. 8(b) shows that there is a sharp peak, indicating a delicate change of stopband pattern as the spectral valley of TL is rather close to TL_{cr}. Fig. 8(c) shows that the lower frequency limit f_1 increases with T.

Fig. 9 shows the spectral changes from the optimal value of $T = 0.485$ (thick solid curves) to its two neighbouring points of $T = 0.42$ (thin solid curves) and $T = 0.56$ (dashed curves). In order to facilitate identification of frequency ranges in different graphs, the three spectral peaks of the optimal tension are marked in all subfigures as open circles. The fundamental changes that take place as T varies is the structural impedance term $(T/\mathrm{i}\omega)(j\pi/L)^2$, where j is the modal index. Because the impact on the higher order modes, such as $j = 3, 4$, is higher than that of lower order modes of $j = 1, 2$, and because there is complicated coupling among all odd modes and among all even modes, the details of modal reactance is not analyzed here. Instead, only the pattern of odd and even modes spectra are shown. The easier way to understand the pattern shift is by asserting that the pattern must shift in such a way that tends to make $T/\mathrm{i}\omega$ a constant. In other words, as T reduces, the pattern shifts to lower frequency, vice versa. This conclusion is evident for most parts of the subfigures in Fig. 9. Fig. 9(a) shows that there is more significant impact of this shift in the region of higher frequencies than lower frequencies. This is so because the total reactance of the coupled system is dominated by the cavity stiffness in low frequencies for the odd modes. On the contrary, the cavity presents virtual radiation mass for the even modes, shown in Fig. 9(b),

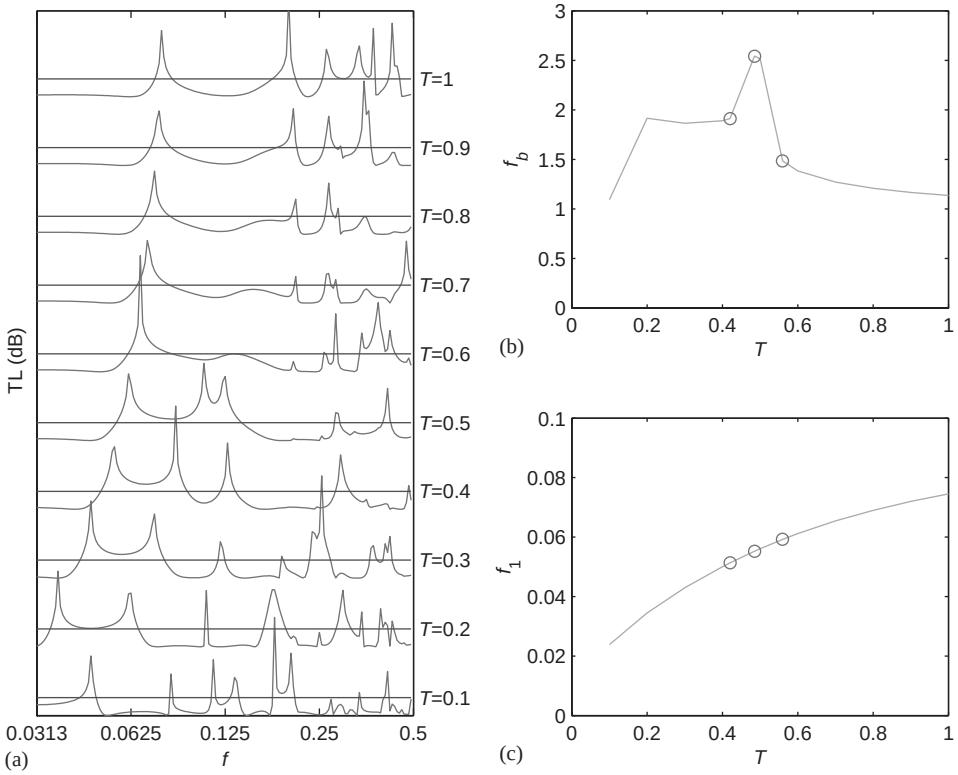

Fig. 8. Variation with tension: (a) the stacked view of transmission loss with tension marked on the right-hand side and horizontal solid line as TL_{cr}; (b) the peak performance in terms of bandwidth; (c) the lower-frequency limit of the stopband. The open circles in (b) and (c) correspond to the cases to be analyzed in the next figure, for which $T = 0.42$, 0.485 and 0.56, respectively.

and the influence of structural parameter is more pronounced in the region of low frequencies. The frequency shift of the first spectral peak shown in Fig. 9(d) follows naturally from this analysis. The changes in the second and third peaks are more complicated as the pattern of the interference index, shown in Fig. 9(c), does not follow the simple rule of frequency shift around and beyond the second spectral peak. As shown in Fig. 9(d) for $T = 0.56$ (dashed curve), the second peak simply disappears. The reason is found in Fig. 9(c) where the value of the interference index drops dramatically from almost 0 (non-interference) to a negative value (cancellation). The even modes do have a finite magnitude beyond the second peak, as shown in Fig. 9(b). For the same reason, the third peak is drastically cut in magnitude due to the cancellation of the rising even modes contribution by the more persisting odd modes contribution. Also shown in Fig. 9(d) is the lack of shift for the third peak for membrane of lower tension $T = 0.42$. The increased interval between the second and third peaks of the thin solid curve results in a deep valley leading to the breaking up of the stopband as defined earlier. The third peak is insensitive to the change in T. This is so because TL is dominated by the even modes contribution and there is no odd modes cancellation as is the case for higher tension. In conclusion, there is a delicate balance between the sound reflections caused by the odd and even modes, and an optimal tension can be found to

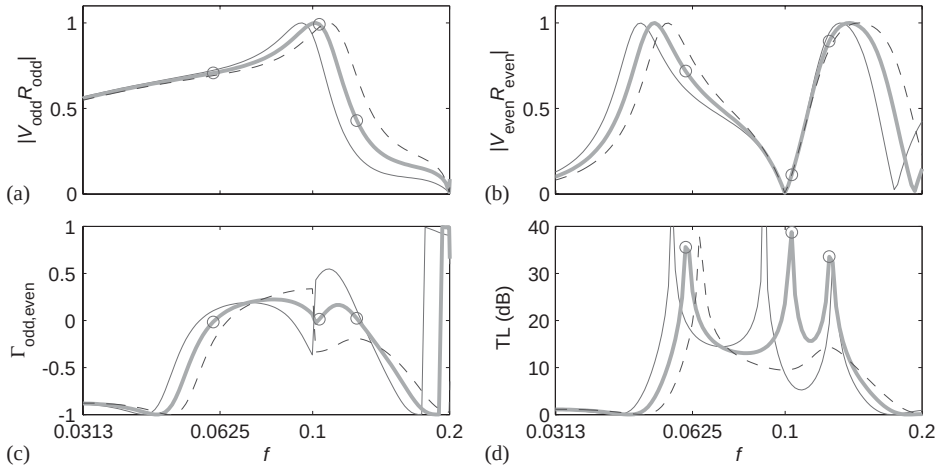

Fig. 9. Modal reactance analyses for the optimal tension and its two neighbouring points shown as open circles in Fig. 8. The thin solid curves are for $T = 0.42$, the thick solid curves are for the optimal tension $T = 0.485$, and the dashed curves are for the higher tension $T = 0.56$. The sub-figures in the left column describe the modal interaction between the odd modes of indices 1 and 3. The second column is for the even modes of indices 2 and 4. The right column is for the overall performance. The open circles on the thick curves mark the frequencies where the membrane under the optimal tension experiences peak performance, $f = 0.604, 0.1033, 0.1250$.

smooth out the final transmission loss for the widest possible stopband. The pivotal role played by the membrane tension is rooted in the fact that the cavity presents different nature of impedance for the odd and even membrane vibration modes.

4.2. Membrane and cavity damping

The effect of membrane damping is illustrated by increasing σ from 0 to $\sigma = 0.1$ for the membrane stretched by the optimal tension $T = 0.485$. The results are compared with that of adding sound absorption material in the cavity. Fig. 10(a) shows the spectral comparison between the lossless membrane (solid curve) and the lossy membrane (dashed curve) with empty cavity.

Apart from the improved performance in the region of high frequencies, the only significant effect is the smearing of the spectral peaks in the stopband. The net effect of this smearing is that TL is reduced at the frequencies of TL peaks. Furthermore, there is no improvement at the TL troughs, contrary to what one might have expected. This is so because the damping mechanism itself reduces the membrane response. Fig. 10(b) compares the spectra of the lossless cavity (solid curve) with cavities filled with different densities of sound absorption materials. The membrane itself is stretched under tension $T = 0.485$ and there is no membrane damping in this subfigure. When the sound absorption material has a very low value of $R_{sam} = 0.025$, the effect is seen to smooth out the spectrum. Notice that, unlike in Fig. 10(a), there is some gain of TL between the second and third peaks. When the flow resistivity is increased further, the spectral pattern makes a transition from the membrane domination to the normal duct lining with resonant peaks caused by the rigid cavity walls. The low-frequency performance for cavity with high value of R_{sam} is not good. In conclusion, neither membrane damping nor sound absorption material filled in the cavity benefits the low-frequency performance of a drum silencer.

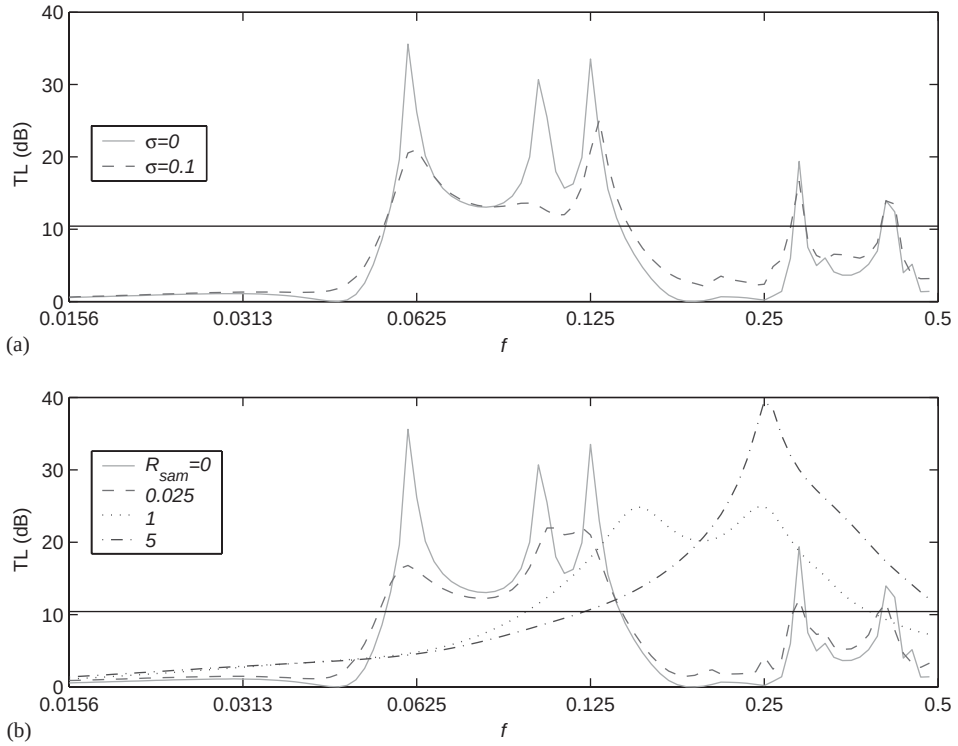

Fig. 10. Effect of (a) membrane damping and (b) sound absorption material inside the cavity. The solid curves are for the membrane under the optimal tension without any damping mechanism.

4.3. Membrane mass

The effect of membrane mass is shown in Fig. 11 for the range of membrane tension of $[0.1, 1]$. The general trend is that the spectra of heavier membranes are shifted towards the lower frequencies compared with light membranes. However, the shift does not necessarily mean a better overall performance in the low-frequency region for heavier membranes since the dips between the peaks tend to be more serious. For example, the membrane with $m = 1$ (thin solid curves) attains its best performance around $T = 0.5$ shown at the top of the left column, where the heavier membrane of $m = 3$ has serious dip between the second and third peaks. This dip is only lifted up at a higher value of tension $T = 0.8$ shown in the middle of the right column. f_1 for the heavy membrane at this tension is actually higher than the value of f_1 for the light membrane at $T = 0.5$. It can be shown that, for even heavier membranes, the dip between the second and the third peaks cannot be lifted up by increasing the value of tension. As a result, the narrow, two-peak stopband achieved with a low value of tension becomes the optimal performance.

The optimal performance for membranes of different mass is shown in Fig. 12. The specification of $m = 0$ does not cause any singular change since the air already imposes radiation virtual mass on the membrane. As shown in Fig. 12(a), the optimal tension, T_{opt}, increases with m. The very linear increase in the initial stage means that the total structural impedance $mi\omega - T(j\pi/L)^2/(i\omega)$ remains more or less unchanged. This result reflects the fact that the optimal

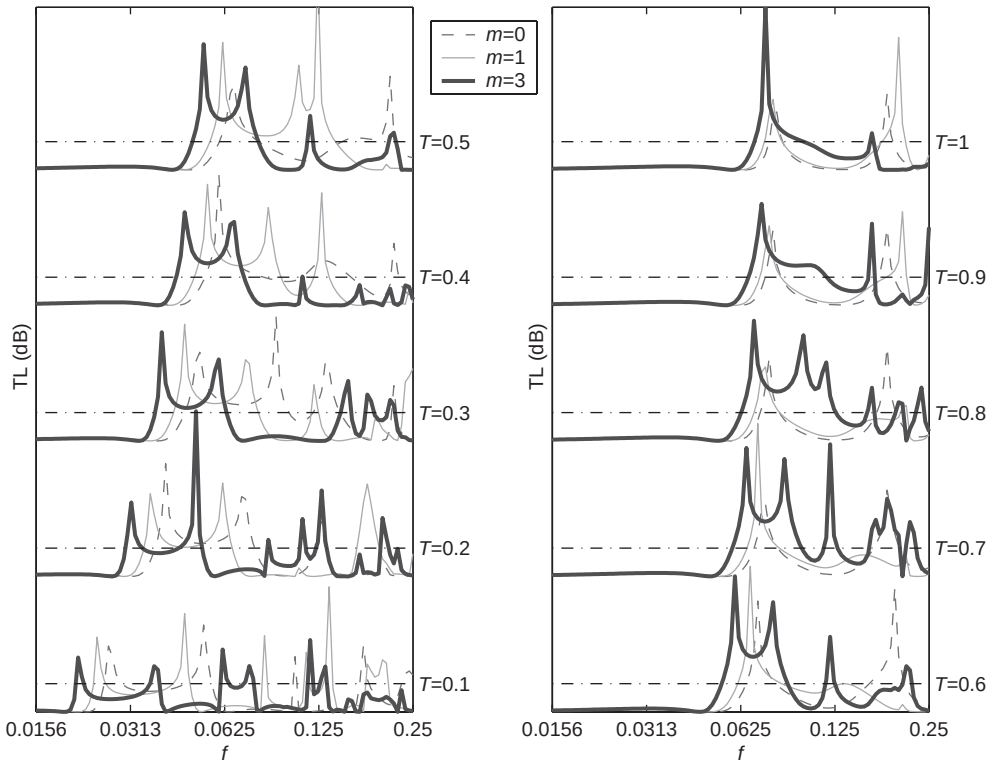

Fig. 11. Spectral variation with membrane tension for different mass.

bandwidth is a result of delicate coupling between the membrane dynamics and the cavity acoustics. A fixed cavity calls for a rather constant membrane behaviour in terms of structural impedance. Fig. 12(b) shows that the lower frequency limit f_1 actually increases. This is somewhat against the physical intuition that resonant frequency decreases with system mass. This outcome is caused by the fact that f_1 is mainly determined by the coupled resonance of the second mode for which the cavity presents radiation mass. As m increases, the change in the system mass is not as great as the change in system stiffness derived solely from the structural tension. The result is an increased resonant frequency for the second mode. Fig. 12(c) shows a steep decrease of bandwidth with m. This is consistent with the definition of $f_b = f_2/f_1$. The critical mass beyond which there is only narrow, twin-peak stopband is shown to be around $m = 6$. The simple conclusion is that, when optimal tension is applied, light membranes are better than heavier membranes both in terms of the lower frequency limit and the logarithmic bandwidth.

5. Conclusions

The essential module of a drum silencer simply consists of a thin membrane tightly stretched over a rectangular cavity which is typically shallow and slender. The grazing incident sound excites the membrane like a drum whose vibration reflects the intruding sound. The module is

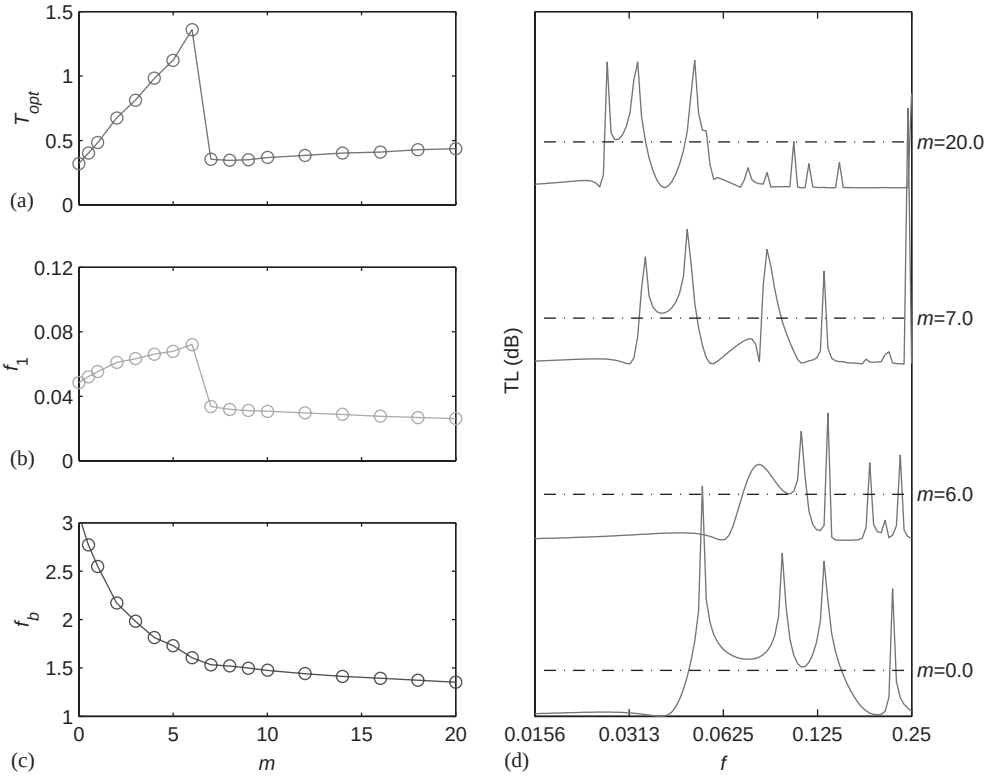

Fig. 12. The optimal parameters (a–c) as functions of membrane mass m, and optimal spectra (d) for three typical values of m.

purely reactive, and a rather broadband performance is predicted. This study focuses on the effects of cavity shape and the membrane properties. It is found that:

1. If the criterion for a good-performance drum silencer is set as the peak transmission loss of an expansion chamber which has cavities with aspect ratio of $\chi = L/h_c = 2$ and with volume three times that occupied by the drum silencer, $TL \geqslant TL_{cr}$, a drum silencer with suitable cavity shape can satisfy this criterion with a wide stopband $[f_1, f_2]$. The stopband begins from a lower frequency limit f_1 for which the membrane length is roughly a quarter-wavelength. The bandwidth normally exceeds one octave and approaches $f_2/f_1 = 3$ for the case with the total volume of $\Lambda = 10$ and with vanishing membrane mass.
2. The performance of a drum silencer is compared with that of traditional duct lining. The optimal cavity shape required of a duct lining is much deeper than that for a drum silencer. The lowest possible f_1 for duct lining is typically higher than that of a drum silencer. The comparison of the low-frequency performance becomes more and more favourable for the drum silencer as the total cavity volume increases, the two being equivalent with a volume of 5 (2.5 for each cavity) for the particular membrane design.
3. For a drum silencer, the TL spectrum becomes wider as the cavity shape becomes slender. The frequency interval between spectral peaks increases and, as a result, the dip between adjacent

peaks would fall below TL_{cr}. On the other hand, a deeper cavity leads to narrower interval between spectral peaks. The stopband is narrower but the higher value of TL at the dip points compensates somewhat for the loss of bandwidth. This gradual spectral shift is found to be mainly caused by the radiation stiffness inside the cavity, while the reflection stiffness plays a minor role.

4. There exists an optimal membrane tension so that a drum silencer of certain geometry can obtain the widest stopband as defined by the triple-volume criterion of $TL \geqslant TL_{cr}$. In order to achieve a wide stopband, the responses of the odd and even modes have to ascertain a certain supplementary spectral relationship. The effect of changing tension is its balance act between the responses of the odd and even modes to incident sound waves.
5. The effect of membrane damping is seen to smooth out the TL spectrum but it does not widen the stopband. If fluffy sound absorption material is added inside the cavities, performance at the higher frequencies improves but that at the lower frequencies suffer. Again, best low-frequency performance is found without any damping inside the cavities.

Acknowledgements

The author thanks the Hong Kong Polytechnic University for its support through project A-PC03.

References

[1] H.V. Fuchs, Alternative fibreless absorbers—new tools and materials for noise control and acoustic comfort, ACUSTICA 87 (2001) 414–422.
[2] L. Huang, A theoretical study of duct noise control by flexible panels, Journal of the Acoustical Society of America 106 (1999) 1801–1809.
[3] S. Brown, Acoustic design of broadcasting studios, Journal of Sound and Vibration 1 (1964) 239–257.
[4] R.D. Ford, M.A. McCormick, Panel sound absorbers, Journal of Sound and Vibration 10 (1969) 411–423.
[5] K. Sakagami, D. Takahashi, H. Gen, M. Morimoto, Acoustic properties of an infinite elastic plate with a back cavity, ACUSTICA 78 (1993) 288–295.
[6] D. Takahashi, K. Sakagami, M. Morimoto, Acoustic properties of permeable membranes, Journal of the Acoustical Society of America 99 (1996) 3003–3009.
[7] K.V. Horoshenkov, K. Sakagami, A method to calculate the acoustic response of a thin, baffled, simply supported poroelastic plate, Journal of the Acoustical Society of America 110 (2001) 904–917.
[8] I. Bosmans, W. Lauriks, G. Lombaert, J. Mermans, G. Vermeir, Sound absorption of stretched ceilings with an impervious synthetic membrane, Journal of the Acoustical Society of America 106 (1999) 233–239.
[9] U. Ackermann, H.V. Fuchs, N. Rambausek, Sound absorbers of a novel membrane construction, Applied Acoustics 25 (1988) 197–215.
[10] J. Kang, H.V. Fuchs, Predicting the absorption of open weave textiles and micro-perforated membranes backed by an air space, Journal of Sound and Vibration 220 (1999) 905–920.
[11] L. Huang, Modal analysis of a drumlike silencer, Journal of the Acoustical Society of America 112 (2002) 2014–2025.
[12] Y.S. Choy, L. Huang, Experimental studies of a drumlike silencer, Journal of the Acoustical Society of America 112 (2002) 2026–2035.
[13] P.E. Doak, Excitation, transmission and radiation of sound from source distributions in hard-walled ducts of finite length (I): the effects of duct cross-section geometry and source distribution space-time pattern, Journal of Sound and Vibration 31 (1973) 1–72.
[14] F.P. Mechel, I.L. Ver, Sound-absorbing materials and sound absorbers, in: L.L. Beranek, I.L. Vér (Eds.), Noise and Vibration Control Engineering, Principles and Applications, Wiley, New York, 1992, Chapter 8.